ChemCatChem

Research Article
doi.org/10.1002/cctc.202201021

Chemistry Europe
European Chemical Societies Publishing

www.chemcatchem.org

# Effect of Steaming on Waste-Derived Zeolite ZSM-5 as Methanol-To-Hydrocarbons Catalyst

Nikolaos Nikolopoulos,[a] Oscar van Veenhuizen,[a] and Bert Marc Weckhuysen*[a]

The valorization of low-grade industrial residues into valuable materials has been a way to reduce the impact of the industry on planetary boundaries. Silicon-rich wastes have been used for zeolite synthesis while the impurities originating from wastes have a vital role in the physicochemical properties and the catalytic performance of waste-derived zeolites. Here, the effect of steaming and the impact of impurities on waste-derived zeolites were investigated. Steamed waste-derived zeolite ZSM-5 maintained their structure while their Brønsted acidity was decreased significantly due to dealumination. Electron paramagnetic resonance revealed that steaming of the samples resulted in the re-dispersion of Fe impurities phases. The waste-derived zeolites exhibited a high amount of weak and intermediate acidity upon steaming. Interestingly, the waste-derived sample with a higher amount of impurities had an increase in Lewis acidity upon steaming, while catalytic testing in the Methanol-to-Hydrocarbons reaction exhibited 10% higher conversion and 4% in propylene yield.

## Introduction

Over the last decades, due to the large and increasing amount of industrial waste, there is a lot of attention in the use of waste streams, such as waste from metallurgical and incineration plants. These types of waste streams can be harmful to human health, as they can react with water and oxygen when exposed to atmospheric conditions, producing acidic wastewater and salts, such as sulfates.[1–3] Establishing a new way to upgrade such waste streams into value-added material could help decrease waste landfilling, but also it could help the transition towards a more circular economy.

Precious and economically important metals can be extracted from waste streams (e.g., flotation tailings from metallurgical industries), while the residual matrix can be utilized to manufacture adsorbents and solid catalysts.[3–5] Research has focused on valorizing silicon-rich wastes (e.g., fly ash and coal fly ash) as a precursor for synthesizing waste-derived heterogeneous catalysts. Fly ash is being commonly used in numerous studies as catalytic support.[6–10] During this study, the term "waste-derived" will be used to refer to materials (i.e., silica, zeolite, and/or catalyst materials) for which silicon-rich wastes from industrial processes are used as precursors. Furthermore, there are other "waste" sources that can be used as precursors for zeolite and/or catalyst synthesis, such as discarded spent catalysts.[11–19] However, the latter type of waste is beyond the scope of this study.

Porous materials, such as MCM-41, Al-MCM-41, and SBA-15, have been synthesized from coal fly ash and used as catalyst materials in different chemical reactions.[4] Waste-derived silica aerogel and adiabatic foam were synthesized using the same type of wastes.[4] Furthermore, many studies show the possibilities of using waste materials to synthesize a variety of different zeolites and zeotypes (e.g., zeolite Y (FAU), X (FAU), ZSM-5 (MFI), SAPO-34 (CHA), A (LTA), P (GIS), and phillipsite (PHI)).[4,20] Missengue *et al.* focused on the transformation of South African coal fly ash into zeolite ZSM-5 as well as its catalytic application to Methanol-to-Hydrocarbons (MTH) reaction.[21] In a second study of the same group, different Structure-Directing Agents (SDAs) were used to improve the physicochemical characteristics as well as the catalytic performance of coal fly ash-derived zeolite ZSM-5.[22]

However, waste-derived zeolite materials can contain impurities originating from the initial waste, which significantly affect their catalytic performances. Chareonpanich *et al.* reported that metal impurities in waste-derived zeolite ZSM-5 slightly boosted $CO_2$ conversion and increased the yield of $C_2$–$C_3$ hydrocarbons.[23] Another study showed that zeolite Na–X from coal fly ash, containing iron oxide impurities, exhibited improved catalytic performance in the oxidation of Volatile Organic Compounds (VOCs).[24,25] The effect of impurities on the physicochemical properties and the catalytic performance of waste-derived zeolites has been previously studied by our research group. It was shown that an increase in the impurities content, such as Ca, Mg, Na, and Fe, resulted in a decrease in the strong acid sites and had a positive influence on the catalyst stability as well as the yields towards light olefins.[26]

Acidity, topology, and porosity are the main parameters that affect the performance in the MTH process.[27–33] Hydro-

[a] N. Nikolopoulos, O. van Veenhuizen, B. M. Weckhuysen
Inorganic Chemistry and Catalysis
Debye Institute for Nanomaterials Science and Institute for Sustainable and Circular Chemistry
Utrecht University
Universiteitsweg 99
3584 CG Utrecht (The Netherlands)
E-mail: B.M.Weckhuysen@uu.nl

Supporting information for this article is available on the WWW under https://doi.org/10.1002/cctc.202201021

*This publication is part of a joint Special Collection with EurJOC and EurJIC on the Netherlands Institute for Catalysis Research. Please see our homepage for more articles in the collection.*

thermal treatment (steaming) is often used as post-treatment of zeolites in order to change their acidic properties and alter intra-crystalline meso/macro pores due to the removal of Al atoms from the zeolite framework (dealumination). Numerous studies have shown that steaming of zeolites, used as an MTH catalyst, can positively influence the catalytic performance by increasing the lifetime and selectivity towards light olefins.[34–37] Hensen *et al.* studied the effect of severe and mild steaming in acidity and the MTH reaction of zeolite ZSM-5. It was found that severe hydrothermal treatment led to a decrease in framework Al content and subsequently to decreased Brønsted acidity. In catalytic activity, severely steamed zeolite ZSM-5 materials exhibit higher amounts of methanol conversion per Brønsted Acid Site (BAS) and higher selectivity towards light olefins, such as ethylene and propylene.[38]

To the best of our knowledge, the effect of hydrothermal treatments in waste-derived zeolite ZSM-5 materials has not been studied yet. Here, we investigate the influence of steaming on the physicochemical properties and catalytic performances of waste-derived zeolite ZSM-5 materials, focusing on the effect of the impurities on the hydrothermal stability of zeolite ZSM-5 materials. Waste flotation tailings were used to synthesize zeolite ZSM-5 materials with different impurities content. Firstly, the influence of steaming temperature on the physicochemical properties of waste-derived zeolite ZSM-5 materials was evaluated using X-ray Diffraction (XRD) and pyridine adsorption followed by Fourier-Transform Infrared (Py-FT-IR) spectroscopy. Furthermore, two waste-derived zeolite ZSM-5 materials with different amounts of impurities, were hydrothermally treated under the same conditions for different amounts of time and compared with a commercial zeolite. Steaming over time caused a decrease in the number of BAS, while the sample with a higher amount of impurities had an increased number of Lewis Acid Sites (LAS). The latter was ascribed to the re-dispersion of the Fe-impurity phase as well as other metal impurities, which further affected the Lewis acidity. The catalytic activity, lifetime, and light olefins yield of the studied zeolite ZSM-5 materials improved as a result of hydrothermal treatments. This study proves the need for a better understanding of the impurities in waste-derived zeolites, which can improve the valorization of low-grade industrial residues.

## Results and DiscussionOrigin and composition of the zeolite catalysts

In a previous study of our research group, waste flotation tailings from Cu primary production were used to synthesize zeolite ZSM-5.[26] Such waste streams consist of various minerals such as quartz ($SiO_2$), dolomite ($CaMg(CO_3)_2$), calcite ($CaCO_3$), and clinochlore ($(Mg,Fe^{2+})_5Al(Si_3Al)O_{10}(OH)_8$).[3,26,39] X-ray Fluorescence (XRF) analysis showed that waste flotation tailings mainly consist of ~51% of silicon dioxide ($SiO_2$), ~16% calcium oxide (CaO), ~11% magnesium oxide (MgO), and ~3.5% iron oxide ($Fe_2O_3$).[26] It was revealed that using waste flotation tailings as precursor for zeolite synthesis could result in the presence of metal impurities (e.g. Ca, Mg, and Fe) in the waste-derived zeolite materials.[26] The content of such impurities in the waste-derived zeolites are inevitable but they can be reduced. It is shown that the pretreatment steps (e.g. heat and acid treatments) and the adjustment of the pH during $SiO_2$ precipitation are important steps to control the impurities content.[26] However, this procedure is not fully effective in removing entirely the so-called impurities. Here, the same approach was followed.[26] Silica materials are precipitated at pH = 3 and pH = 10 and they are used as precursors for the synthesis of waste-derived zeolites ZSM-5 (denoted as S3 HZSM-5 and S10 HZSM-5, accordingly). The waste-derived samples were compared with a commercial zeolite ZSM-5 (denoted as Com HZSM-5). It was found by ICP-OES analysis of the samples, as summarized in Table 1, that the S3 zeolite sample has a lower amount of impurities than the S10 zeolite sample. It can also be noted that S3 HZSM-5 has comparable levels of Ca and Mg relative to the Com ZSM-5, and also exhibits 0.2 wt% of Fe, while S10 HZSM-5 has an increased amount of Al, Fe, Ca, and Mg. The latter observation can be attributed to the pH change in the silica precipitation step as at pH = 3 only $Fe^{3+}$ precipitate while at pH = 10, divalent metals, such as Mg, Ca, and $Fe^{2+}$ precipitate.[26,40–41]

## Stability of zeolite catalysts steamed at different temperatures

The waste-derived zeolite ZSM-5 (S3 HZSM-5) material was steamed at different temperatures (400–700 °C) for 300 min in order to investigate its hydrothermal stability and understand the effect of the steaming temperature on its physicochemical characteristics. The waste-derived sample was compared with a commercial (Com HZSM-5) zeolite sample. Figure 1(a, b) shows the XRD patterns of the commercial and waste-derived zeolite materials after applying the hydrothermal treatments at 400–700 °C for 300 min. The Com HZSM-5 sample showed great stability under hydrothermal treatments until 500 °C as the XRD patterns had no significant change. However, steaming the sample at 600 and 700 °C resulted in a decrease in the reflections intensity and flattening, implying the damage of the zeolite framework as well as dealumination. Furthermore, inspecting the peak at 2θ equal to 28.3, we can observe a splitting of the peak in two after severe steaming (at temper-

**Table 1.** Overview of the chemical composition of the waste-derived zeolites and the reference zeolite ZSM-5 material. Inductively Coupled Plasma-Optical Emission Spectroscopy (ICP-OES) analysis of commercial zeolite ZSM-5 (denoted as Com HZSM-5) and waste-derived zeolites ZSM-5 obtained at pH 3 (denoted as S3 HZSM-5) and 10 (denoted as S10 HZSM-5).

| Samples | Si[a] | Al[a] | Ca[a] | Fe[a] | Mg[a] |
|---|---|---|---|---|---|
| Com HZSM-5 | 33.7 | 1.92 | 0.065 | 0.01 | 0.04 |
| S3 HZSM-5 | 30.3 | 2.3 | 0.08 | 0.20 | 0.06 |
| S10 HZSM-5 | 26.5 | 3.12 | 0.12 | 0.34 | 0.52 |

[a] Presented in wt%.

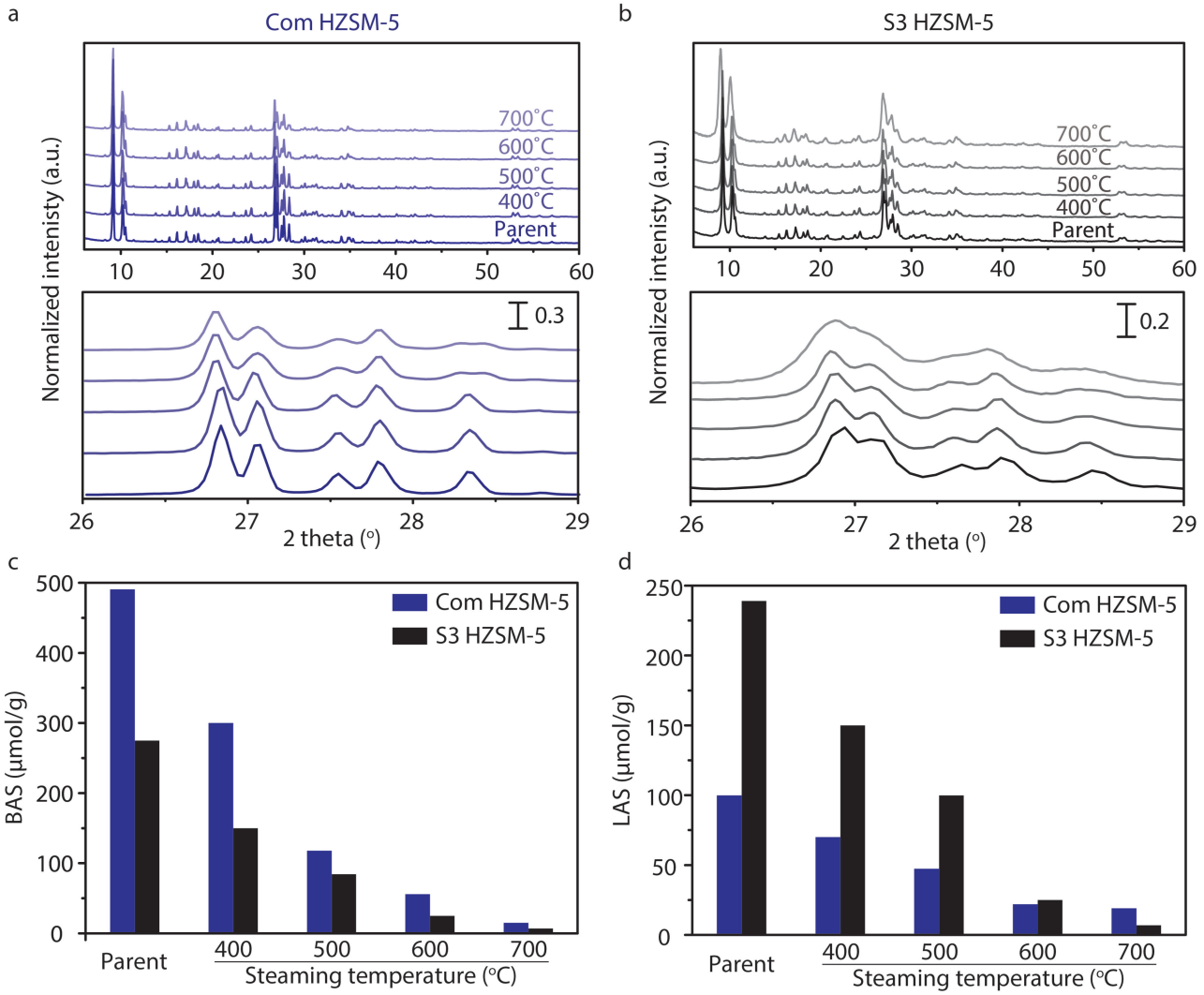


**Figure 1.** Effect of steaming on the structure and acidic properties of waste-derived and commercial zeolite ZSM-5 materials. X-ray Diffraction (XRD) patterns of parent and steamed zeolites for 300 min at 400, 500, 600, and 700 °C for the 2θ 6–60° and 26–29° regions for a) Com HZSM-5 and b) S3 HZSM-5. c) Brønsted Acid Sites (BAS) and d) Lewis Acid Sites (LAS) determined by pyridine adsorption followed by Fourier-Transform Infrared (Py-FT-IR) spectroscopy for the parent and steamed for 300 min at 400–700 °C waste-derived and commercial zeolite ZSM-5 materials.

atures 600 and 700 °C), implying the presence of monoclinic symmetry. This can be attributed to the high temperatures and the degree of dealumination during the steaming process.[42–43] On the other hand, the S3 HZSM-5 sample showed a decrease in the XRD peak intensities and flattening after steaming at 400 °C for 300 min. It can be noted that after steaming at 700 °C for 300 min, the zeolite framework was severely damaged, as broad XRD peaks and severe flattening are observed. The presence of monoclinic symmetry can also be noted in S3 sample. In the parent sample, there is an asymmetry shape of the peak at 28.3°, while in the steamed samples a peak splitting was observed. Overall, the waste-derived zeolite materials showed that they are more prone to framework collapse than the commercial zeolite. This phenomenon can also be attributed to the synthesis method as well as to the experimental parameters followed in this study to prepare these materials. However, the influence of the specific synthesis method is beyond the scope of this study.

Moreover, the acidic properties and their changes upon steaming were also evaluated by Py-FT-IR spectroscopy, as shown in Figure 1(c, d). Comparing the BAS of the two parent samples, their difference can be attributed to the presence of impurities. Fe, Mg, and Ca species can block the acid sites of the waste-derived zeolites, as previously proved by our research group.[26] The waste-derived and the commercial zeolite materials exhibit similar trends in the decrease of the number of BAS, as illustrated in Figure 1c. Even if the commercial sample started from a higher number of BAS, it is worth mentioning that both samples had a comparable amount of BAS after steaming at 700 °C for 300 min. Regarding the number of LAS (Figure 1d), the Com HZSM-5 sample showed a minor decrease by increasing the steaming temperature, while for the S3 HZSM-5 sample decreased from ~99 µmol/g to ~10 µmol/g. This initial

difference of the amount of LAS in the parent commercial and waste-derived zeolites can be explained from the existence of impurities, but also by the formation of Extra-Framework Aluminum (EFAL) in the waste-derived sample.[26]

## Changes on the physicochemical properties of zeolite catalysts upon steaming

In order to further understand the effect of steaming on the physicochemical properties and catalytic performance of waste-derived zeolites taking into account the complexity of the materials due to the incorporation of impurities, we treated the three samples at 500 °C for different steaming times, such as 15, 30, 120, and 300 min.

Figure 2 illustrates the XRD patterns of the parent and steamed samples at 500 °C for time period between 15 and 300 min. In general, as shown in Figure 2 (a, c, and e), all of the samples preserved their framework structure as no significant changes can be noted after steaming. The commercial HZSM-5 sample, of which the XRD pattern is given in Figure 2b, after a close inspection in the 2theta area of 26–29 degrees, showed a slight decrease in peak intensity after 300 min of steaming demonstrating the hydrothermal stability of the sample. However, the waste-derived samples, of which the XRD pattern is given in Figure 2 (d, f), demonstrating a decrease of the peak intensities even in the first minutes of steaming (i.e., 15 min) as well as XRD peak flattening, undergoes zeolite dealumination. These findings align with the observations mentioned above, where waste-derived zeolites are more prone to structural changes due to steaming.

The SEM images, shown in Figure S1, of the waste-derived zeolites and the commercial ZSM-5 materials, show the morphology of the samples. Figure S1a illustrates that Com HZSM-5 consists of typical coffin-shape crystals with the size of 1–5 μm along the *c*-axis. On the contrary, the waste-derived zeolite samples showed different morphology. S3 HZSM-5, as shown in Figure S1b, consists of small cube-like crystals which agglomerate in spherical particles with the size of 0.5–5 μm. Moreover, S10 HZSM-5, as shown in Figure S1c, consists of small sheet-like crystals which agglomerate in spherical particles with the size of 2–10 μm. Overall, the differences in the morphology of the waste-derived zeolite materials can ascribed to the impurities content of the samples. Na, Ca, Mg, and Fe cations act as inorganic structure directing agent as well as framework-charge compensation cations. The latter can justify the changes in the morphologies of the waste-derived zeolite materials.[44] Furthermore, it is shown in the open literature that the crystal size and crystallization step during zeolite synthesis can be influenced by the substitution of Na cations with other alkali metals.[45–47] The same trends were also demonstrated from our previous study on the impact of impurities on the waste-derived zeolite materials.[26] Ar physisorption measurements

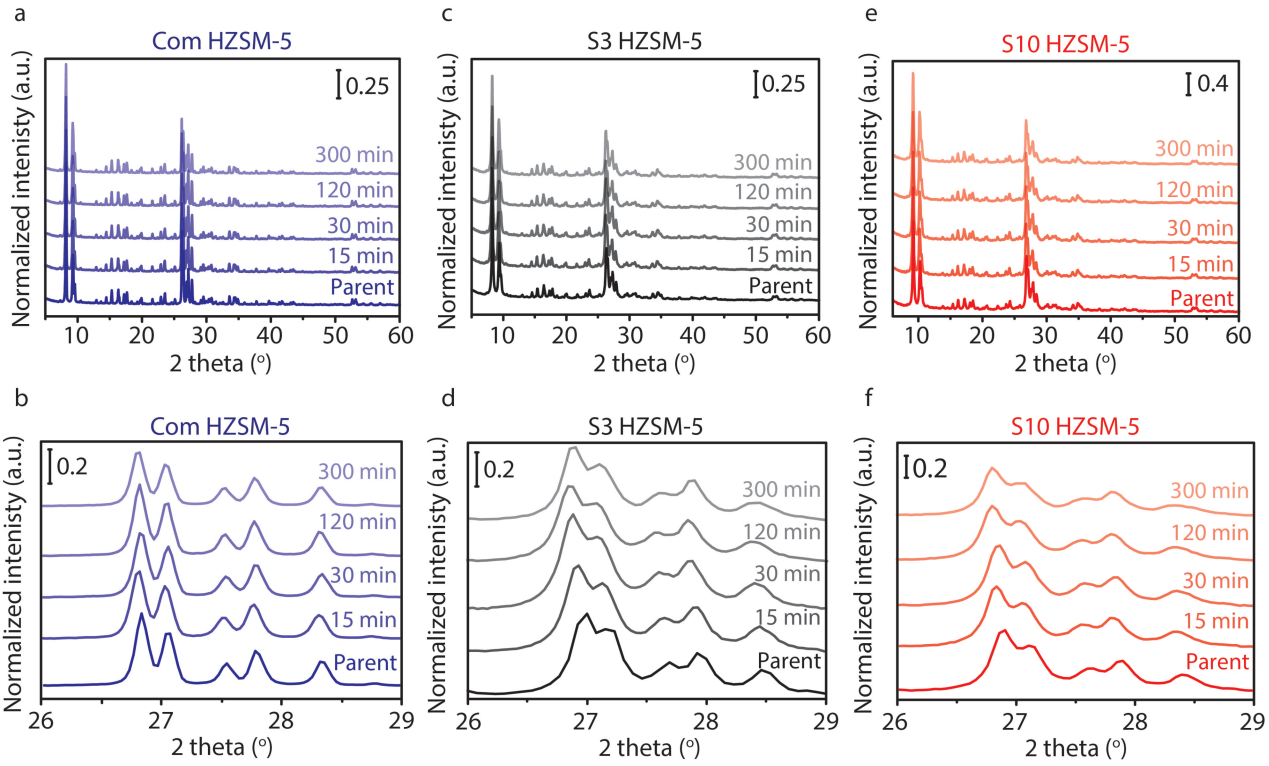


**Figure 2.** Structural changes of waste-derived and commercial zeolite ZSM-5 materials as a function of steaming time. X-ray Diffraction (XRD) patterns of the parent and steamed zeolites for 15, 30, 120, and 300 min at 500 °C for the 2θ 6–60° (a, c, e) and 26–29° (b, d, f) regions for Com HZSM-5 (a, b), S3 HZSM-5 (c, d), S10 HZSM-5 (e, f).

reveal the textural properties of the samples under study, as shown in Fig S2 and Table S1. Figure S2a illustrates that Com HZSM-5 exhibit a type I isotherm, which corresponds to a microporous material with small external surface. Com HZSM-5 steamed for 300 min at 400 °C exhibited a hysteresis loop.[48] The latter observation suggests the formation of mesopores during steaming as it is also shown in the pore volume distribution (Figure S2b). Moreover, Figure S2b show the collapse of micropores during steaming. Both waste-derived zeolite materials (i.e., S3 HZSM-5 and S10 HZSM-5) exhibit a combination of type I and II isotherms which is characteristic for agglomeration of zeolite crystals and/or mesoporous zeolites.[48]

After steaming treatment for 300 min at 400 °C of the waste-derived zeolite materials, collapsing of micropores and formation of larger pores is observed, as shown in Figure S2(c–f). As summarized in Table S2, steaming treatments resulted in a decrease in the Specific Surface Area (SSA) of all samples under study.

The EPR spectra of samples S3 HZSM-5 and S10 HZSM-5 are shown in Figure 3(a, b), respectively. Sample S3 and S10 showed three different EPR signals at g-values of 2.1, 4.3, and >6. The EPR signal at g = 4.3 is assigned to isolated $Fe^{3+}$ species in tetrahedral coordination, which can be Fe species in the framework or extra-framework species in a zeolite structure. On top of that, an EPR signal at ~g >6 can be observed, which is related to the presence of isolated Fe species with higher coordination numbers. Regarding the g = 2 EPR signal, six weaker lines can be observed. These features can be assigned to the hyperfine structure of paramagnetic $Mn^{2+}$ species.[49] Indeed, $^{55}Mn$ has a nuclear spin (I) of 5/2, which will couple with the electron spin, leading to 6 sublevels. In addition, since $^{56}Fe$ is the most common isotope (92%) and has a spin of 0, this hyperfine structure cannot be due to the presence of Fe. These $Mn^{2+}$ species can originate from the initial waste flotation tailings and can be easily detected by EPR spectroscopy even in trace amounts. Hydrothermal treatment of waste-derived zeolite ZSM-5 materials caused a re-dispersion of Fe impurities as the relative intensity ratio between the lines at ~4.3 and >6 changes. The latter observation is translated to the fact that the S3 sample appears to have more Fe species with higher coordination numbers while the S10 sample shows the presence of Fe species in the framework or extra-framework species in a zeolite predominantly.

The $NH_3$-TPD analysis, as shown in Figure 4(a–c), was performed to probe the strength and the total amount of the acid sites before and after steaming the commercial and waste-derived zeolite ZSM-5 materials. Two major peaks centered at ~230 °C and ~430 °C were recorded for the parent commercial sample, while the parent waste-derived samples showed two major peaks at ~200 °C and ~400 °C. The peak at ~200 °C and/or ~250 °C can be assigned to weak acid sites, while the peak at ~400 °C and/or ~430 °C can be attributed to strong acid sites.[26,50,51] The commercial sample has a higher amount of acid sites than the waste-derived samples mainly due to impurities in the waste-derived samples, as previously proved in literature.[26] Upon steaming, there is a decrease in the acidity of the commercial and waste-derived samples under study. Furthermore, the peaks are shifted to lower temperatures, implying the weakening of the acid sites due to the hydrothermal treatment. To further understand the effect of steaming in the acid sites of the zeolite materials, the $NH_3$-TPD curves were deconvoluted, taking into account the presence of three different types of acid sites (i.e., weak, intermediate, and strong) and the amount of each category was plotted versus steaming time, as shown in Figure 4(d–f). The commercial sample showed a decrease of the number of acid sites over time upon steaming in every category. However, the waste-derived samples showed resistance in the decrease of the number of the weak and intermediate acid sites. Specifically, S10 samples, which have a higher amount of impurities, have also a higher amount of

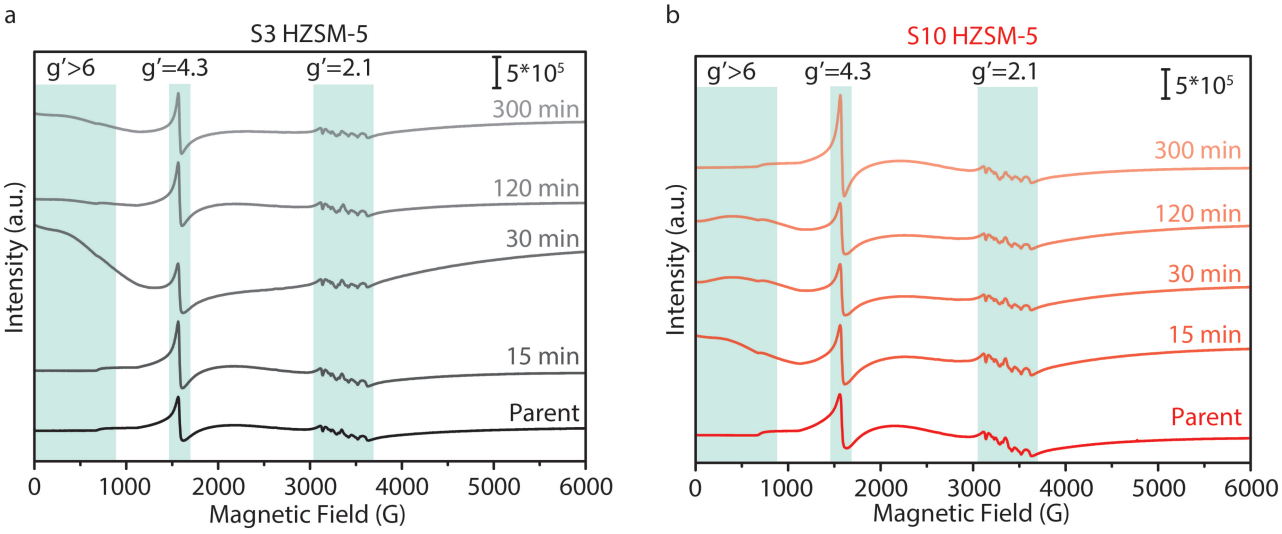


**Figure 3.** Evolution of Fe species in waste-derived zeolite ZSM-5 materials after hydrothermal treatment. Electron Paramagnetic Resonance (EPR) spectra for a) S3 HZSM-5 and b) S10 HZSM-5 before and after hydrothermal treatment.

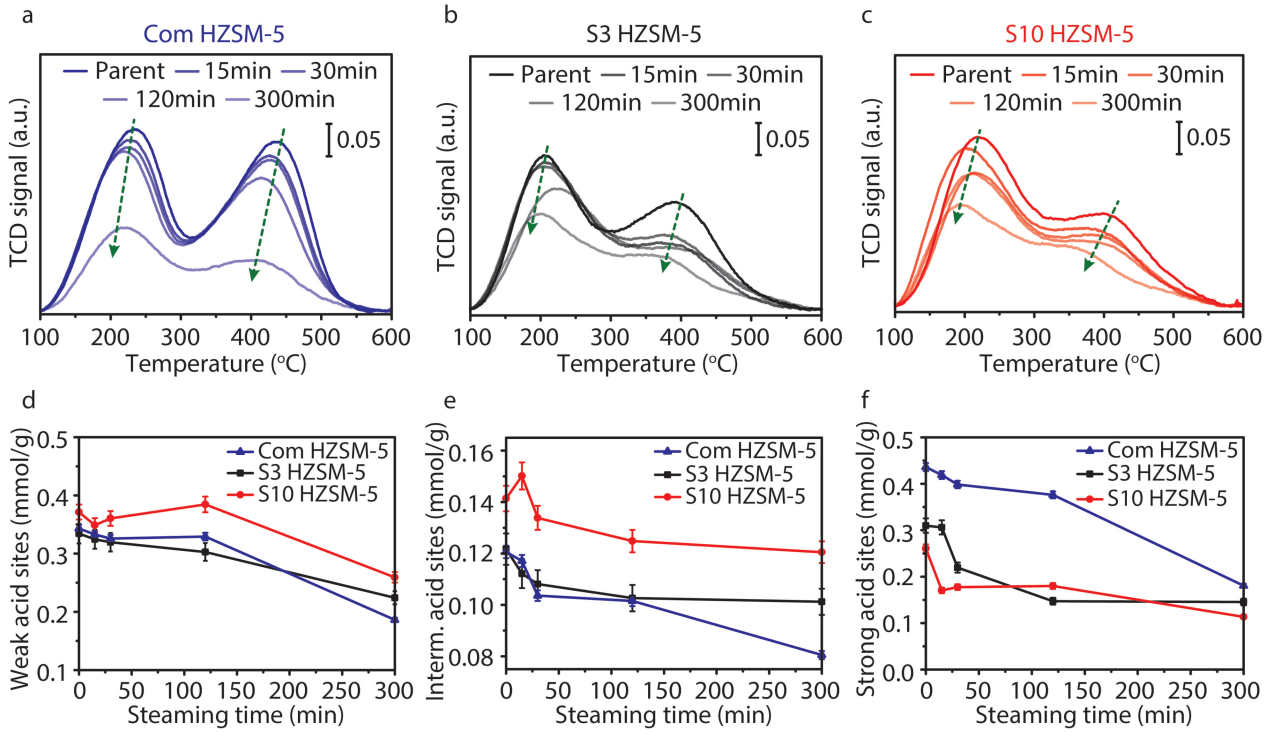


**Figure 4.** Changes in the amount and strength of the acid sites upon steaming. Ammonia Temperature-Programmed Desorption ($NH_3$-TPD) analysis of a) the commercial sample (blue), b) S3 (black), and c) S10 (red) sample before and after steaming. d) Weak, e) intermediate, and f) strong acid sites calculated by deconvolution of $NH_3$-TPD analysis of each sample and plotted versus the temperature of hydrothermal steaming (steaming time).

weak and intermediate acid sites. Regarding the intermediate acid sites, it appears to increase for short steaming periods and decrease for longer steaming times (i.e., 30–300 min). It is also noted that weak acid sites are maintained upon steaming treatments for up to 120 min. Overall, it is expected that steaming leads to decrease of all types of acid sites. However, this phenomenon can be attributed to the weakening of strong acid sites during such short steaming times.

As shown in Figure 5, Py-FT-IR spectroscopy was performed for all samples under study to evaluate further the nature of the acid sites and their changes after hydrothermal treatment. The peaks at 1453 $cm^{-1}$ and 1545 $cm^{-1}$ are assigned to LAS and BAS, respectively.[52–54] The commercial zeolite sample upon steaming showed a strong decrease in the number of BAS as well as a slight decrease in the number of LAS. Regarding the waste-derived zeolite ZSM-5 materials, especially, sample S3 showed the same trend as the commercial sample. On the contrary, sample S10, which contains a high amount of impurities, showed a decrease in the number of BAS, while the number of LAS showed a remarkable increase. It is known from the literature that steaming could create some LAS due to the formation of a group of EFAL species.[38,55] However, there is no clear correlation of the number of LAS and the extra-framework species, but also, in our case, the extent of this increase of LAS acidity in sample S10 could not only be justified from the transformation of framework Al to extra-framework Al. The latter assumption is also confirmed because the commercial sample and the sample S3, with low impurities, did not show any increase in LAS upon hydrothermal treatments. As shown in Table 1, ICP-OES revealed ~1 wt% of impurities, such as Fe, Ca, and Mg, present in the sample S10 HZSM-5. As shown in Figure 5c, there is a shift of the peak at 1453 $cm^{-1}$, corresponding to LAS, to lower frequencies (1445 $cm^{-1}$) upon steaming of the S10 sample which implies the presence of new medium in strength LAS.[56–58] The latter is in line with the literature in which metal modified zeolites present the same phenomena and peak shifts in Py-FT-IR spectroscopy experiments attributing them to the formation of new LAS due to metal incorporation in the zeolites.[56–58] Specifically, Fermoso *et al.* studied the modification of zeolite ZSM-5 catalyst materials with Mg and Zn.[57] It is reported that the peak at 1456 $cm^{-1}$ corresponding to LAS are shifted to lower frequencies (i.e., 1448 $cm^{-1}$) upon addition of Mg. Considering all the above mentioned, it seems that the presence of these impurities during steaming at elevated temperatures in the presence of water could result in the formation of new LAS. This phenomenon is also supported by the EPR results (Figure 3) where it is evident that there is a re-dispersion of the Fe-impurity phase upon steaming. $NH_3$-TPD results for sample S10 (Figure 4) showed higher amount of weak and intermediate acid sites that it could also be attributed in the formation of these new LAS.

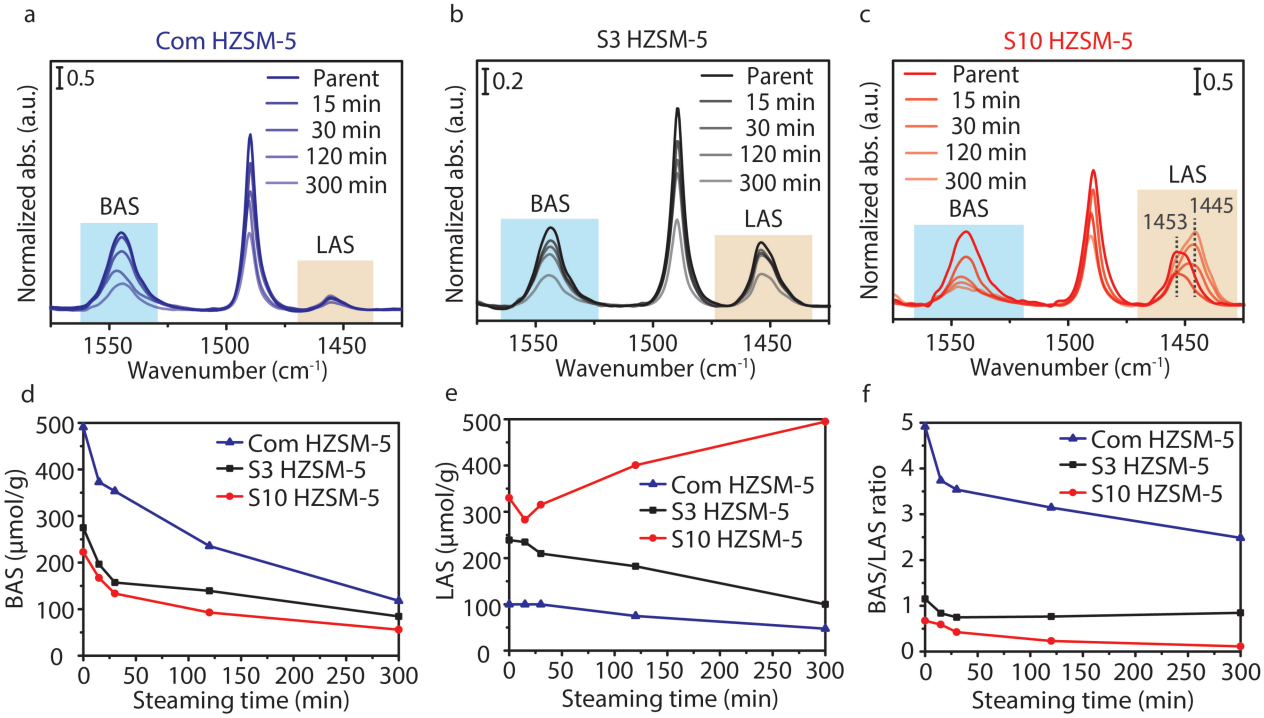


**Figure 5.** Effect of impurities on the modification of Brønsted and Lewis acidity in waste-derived and commercial zeolite ZSM-5 materials as a function of the steaming time. Pyridine adsorption followed by Fourier-Transform Infrared (Py-FT-IR) spectroscopy at 150 °C of a) the commercial sample (blue), b) S3 (black), and c) S10 (red) before and after steaming. d) Brønsted Acid Sites (BAS), e) Lewis Acid Sites (LAS), and f) BAS/LAS calculated from the Py-FT-IR spectra of each sample and plotted versus the steaming time.

## Linking hydrothermal stability, physicochemical properties, and catalytic activity

Figure 6 illustrates the results of the MTH tests performed for the three parent zeolite samples and the 15 min, 120 min, and 300 min steamed samples. Regarding the commercial sample (Figure 6a), it exhibited almost complete methanol conversion for 150 min, and then it started deactivating rapidly, reaching ~60% conversion after 1000 min Time-on-Stream (TOS). A short-time hydrothermal treatment (15 min) leads to a slower deactivation after ~150 min TOS, thereby reaching ~83% methanol conversion. Increasing the steaming time to 300 min resulted in a high methanol conversion (>90%) for at least 1000 min TOS. As shown in Figure 4 and Figure 5, steaming greatly influences the acidic properties of the zeolite materials, causing a reduction of the amount and the strength of the acid sites in the zeolites, which can lead to slower catalyst deactivation. The results mentioned above align with the literature as post-treatments have been shown to lead to prolonged catalyst stability and resistance in the deactivation due to a decrease of the number of strong BAS.[31,35,38,59] Focusing on the formation of light olefins (i.e., ethylene and propylene), as expected, longer steaming times would result in a higher propylene selectivity while it would decrease the ethylene yield. Yarulina *et al.* established the acidity-performance relationship in which a low BAS concentration proved to be the key to achieving high propylene selectivity, while high BAS concentration enhances the ethylene selectivity.[59]

Regarding the waste-derived samples, sample S3 showed similar trends in the conversion and the yields towards light olefins with the commercial sample. However, the waste-derived zeolite with a higher amount of impurities, sample S10, exhibited some differences in methanol conversion compared to the other two samples and a more distinct increase on propylene yield. Longer steaming time (i.e., 120 and 300 min) of the S10 sample led to an increase of ~10% methanol conversion. It is reported in the literature and supported from our study that upon severe steaming and reduced acidity, a decrease of conversion occurs.[38] This dissimilarity can be attributed to the changes of the type and the amount of acidity upon steaming, as shown in Figure 4 and Figure 5. As previously explained, sample S10 showed the formation of a large amount of LAS acidity. Even though the role of LAS in the open literature is often neglected or posed as having a negative influence in the catalytic performance, some studies proved their critical role in the MTH process.[26,59–62] It is worth mentioning that the generation of LAS due to the incorporation of alkaline-earth metals is the key to design a long-living and highly selective towards propylene catalyst.[59,60] Jiao *et al.*, among other researchers, studied the effect of Fe on zeolite HZSM-5 catalyst materials.[63–66] It was shown that upon impregnation of Fe on zeolite HZSM-5 there was an increase on propylene selectivity. Further catalytic tests showed that Fe species could further catalyzed the conversion of propane and

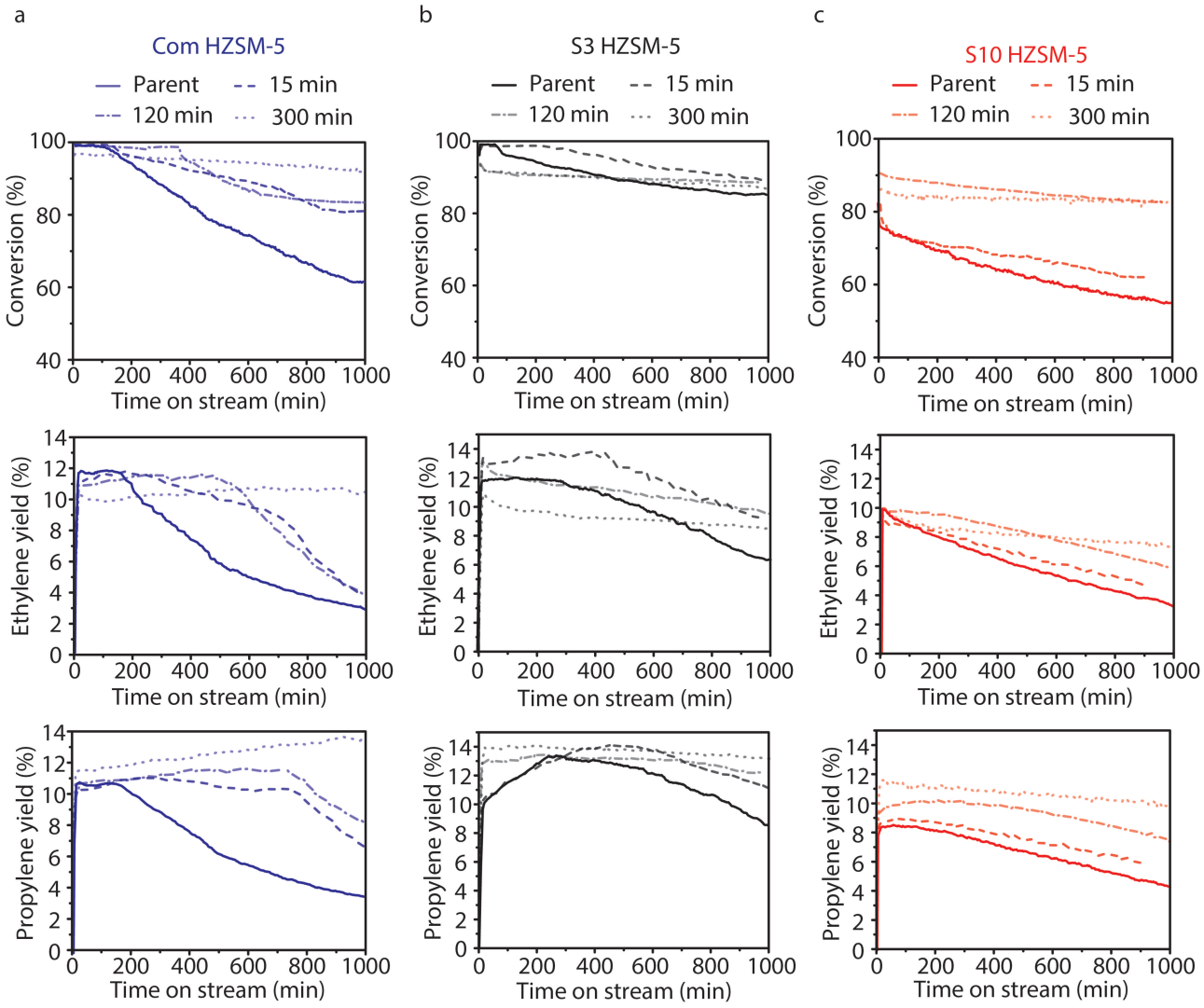


**Figure 6.** Catalytic activity of waste-derived and commercial zeolite ZSM-5 materials in the Methanol-to-Hydrocarbons (MTH) process. Conversion and yields of ethylene and propylene produced versus Time-on-Stream (TOS) of parent Com HZSM-5 (blue), S3 HZSM-5 (black), and S10 HZSM-5 (red) as well as steamed samples at 500 °C for 15, 120, and 300 min.

butylene products towards propylene and methane. The latter in combination with the re-dispersion phenomena of Fe species in the waste-derived zeolites (as shown by EPR results in Figure 3) could also justify the increased propylene yield upon steaming.

## *Operando* spectroscopy during catalysis over zeolite catalysts

*Operando* UV-Vis Diffuse Reflectance Spectroscopy (DRS) was used to better understand the catalytic behavior of the parent Com, S3, and S10 HZSM-5 as well as the steamed samples for 300 min at 500 °C. UV-Vis DRS has shown to be able to differentiate between reaction intermediates and/or Hydrocarbon Pool (HP) species as well as internal and external coke species. Figure 7 illustrates the UV-Vis DRS data that were recorded between 250 and 900 nm. The samples show absorption bands at ~285 nm, ~370 nm, ~420 nm, and >500 nm. These absorption bands can be attributed to polyalkyl-substituted cyclopentadienium ion with four or five alkyl groups (i.e., ~282 nm and ~285 nm), highly methylated areniums and/or aliphatic dienes (i.e., ~367 nm and ~370 nm), two and three-ring neutral polyaromatics and/or ethyl-substituted aromatic species and/or methylated naphthalene carbocations (i.e., ~416 nm and ~420 nm) and, finally methylated polyareniums ions/highly conjugated polyenes (> 500 nm).[61,67–78] As shown in Figure 7(a–c), the S10 sample shows relatively lower aromatic hydrocarbon species, which is related to the lower amount of BAS present in this sample compared to the commercial and S3 parent samples. It is known that BAS promotes hydride transfer reactions, which form aromatic compounds as well as $C_{1-5}$ paraffins.[62,79]

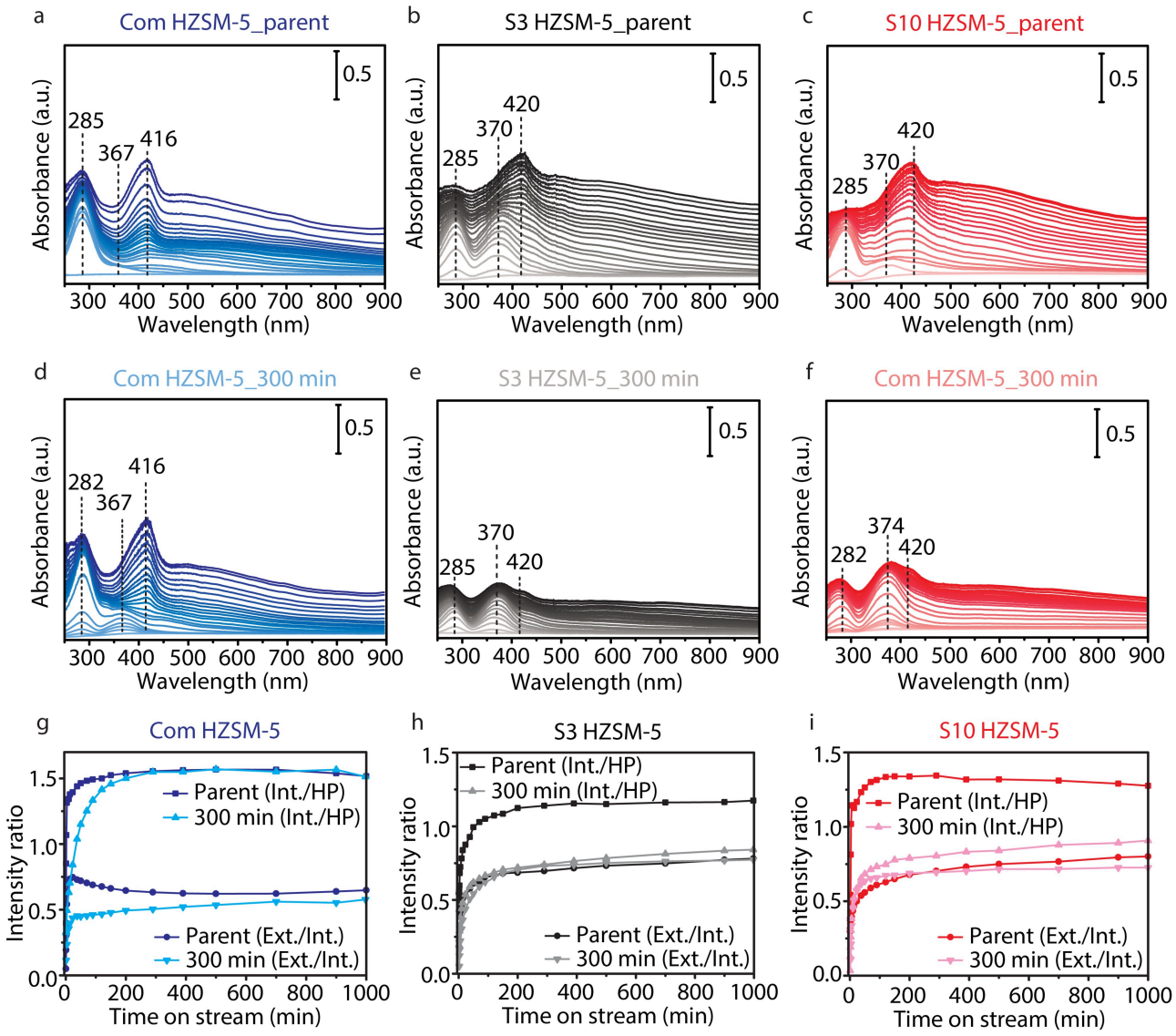


**Figure 7.** Evolution of coke precursors and hydrocarbon pool species. a–c) *Operando* Ultraviolet Visible (UV-Vis) Diffuse Reflectance Spectroscopy (DRS) data of the parent Com HZSM-5 (blue), S3 HZSM-5 (black), and S10 HZSM-5 (red). d–f) *Operando* UV-Vis DRS data of the parent Com HZSM-5 (blue), S3 HZSM-5 (black), and S10 HZSM-5 (red). Changes of the intensity ratio of internal species (~420 nm) to Hydrocarbon Pool (HP) species (~370 nm) and external species (~565 nm) to internal species (~420 nm) versus Time-on-Stream (TOS) of the g) Com HZSM-5 (blue), h) S3 HZSM-5 (black), and i) S10 HZSM-5 (red) (parent samples and steamed samples for 300 min at 500 °C).

Regarding the parent samples, it can be noted that waste-derived zeolite ZSM-5 materials contain a relatively higher amount of poly-condensed aromatic species than the commercial sample, which can be attributed to the different morphologies of the samples. As previously discussed, the Com HZSM-5 has a morphology of cube-like crystals of 1–5 μm, while the waste-derived samples consist of spherical agglomerates of smaller zeolite crystals. Figure 7 (d–f) illustrates the *operando* UV-Vis DRS data recorded for the Com, S3, and S10 samples steamed for 300 min at 500 °C in order to further understand the changes in the reactive intermediates and coke formation induced upon hydrothermal treatments. All samples, after steaming, show no significant shifts in the absorption spectra. However, the relative intensities of the absorption bands changed drastically after steaming.

The temporal changes of the band intensity ratio of internal species (~420 nm) to HCP species (~370 nm) and external species (~565 nm) to internal species (~420 nm) versus TOS of the samples before and after steaming were plotted to visualize the effect of the steaming on the catalytic performances of the materials. It is noted that the parent commercial sample (Com HZSM-5) showed a faster formation rate of internal coke species in respect to HCP species due to the higher amount of BAS which could favor further oligomerization reactions to larger polyaromatic species. The commercial HZSM-5 exhibited a slower formation of internal coke species with respect to the formation HCP species after steaming the material until 200 min

TOS, which the reduced amount of BAS can explain. At the same time, the Com HZSM-5 sample appeared to form less polyaromatic species (e.g., external coke). Hydrothermal treatments can reduce the amount of BAS and induce extra porosity, which prevent reactions to incorporate aromatic moieties.[59,80] The catalytic activity data confirm the latter as the commercial parent sample started to deactivate after less than 200 min TOS when the steamed sample was still active for at least 1000 min TOS. Interestingly, the waste-derived zeolite ZSM-5 materials showed a different catalytic behavior as there was a distinct change in the ratio of the internal coke species to HCP species. It can be seen that the parent samples had a rapid and profound formation of internal coke species (namely naphthalene and/or anthracene) compared to the HCP species. The situation appears completely inverted after steaming the materials as it is evident that the formation of HCP species, with respect to internal species, is now more profound. This phenomenon can also be attributed to the reduced number of BAS, the reduced number of strong acid sites, and extra porosity formed during steaming. As aforementioned, the $NH_3$-TPD measurements showed that the waste-derived zeolite ZSM-5 materials appeared to retain their weak and intermediate acid sites. No significant changes were observed in the ratio between external to internal coke species for the waste-derived samples steaming before and after steaming, thereby proving the effect of the morphology of the zeolite crystals on the formation of external coke species.

## Conclusion

The influence of hydrothermal treatments and the presence of impurities in waste-derived zeolite ZSM-5 materials on the physicochemical properties as well as the catalytic performance in the Methanol-to-Hydrocarbons (MTH) reaction was studied. Zeolite ZSM-5 materials were synthesized using waste from the copper production industry. Firstly, the effect of the steaming temperature was investigated by taking a waste-derived zeolite sample with a relatively low amount of impurities and treating it at temperatures between 400–700 °C for 300 min. The materials were compared with a commercial zeolite ZSM-5 sample. X-ray Diffraction (XRD) showed that even after a long steaming time at elevated temperatures the zeolite framework structure was preserved, while losing most of its acidity. In the next step, aiming to further understand the effect of impurities in a combination of a hydrothermal treatment process, two waste-derived samples with varying impurities content were treated at 500 °C for different times (i.e., 15–300 min). Interestingly, Electron Paramagnetic Resonance (EPR) showed that a re-dispersion phenomenon of Fe phase occurs for the waste-derived samples during steaming. Ammonia Temperature-Programmed Desorption ($NH_3$-TPD) revealed that upon steaming, there is a total decrease in acidity. However, the waste-based zeolite materials showed resistance in the decrease of weak and intermediate acid sites. Pyridine adsorption followed by Fourier-Transform Infrared (Py-FT-IR) spectroscopy studies, which were used to assess the extent of dealumination phenomena and their effect on the acidity, revealed a decrease in the number of Brønsted Acid Sites (BAS) as expected for all three samples after steaming. On the contrary, the waste-derived sample with a higher amount of impurities after 120 and/or 300 min of steaming at 500 °C exhibited a great increase in the number of Lewis Acid Sites (LAS). Parent and steamed samples were tested for their catalytic performance in the MTH reaction. It was found that steaming treatments increased the lifetime of the catalyst materials as well as the yield of propylene. Hence, hydrothermal treatments and impurities content significantly impact the physicochemical properties and catalytic performance of the MTH reaction as a synergistic effect exists.

## Experimental Section

### Chemicals and materials

The following chemicals, gases, and materials were used: ammonium nitrate ($NH_4NO_3$, 97%, Sigma Aldrich), hydrochloric acid (HCl, fuming 37%, Merck), sodium hydroxide (NaOH, 100%, EMSURE), sulfuric acid ($H_2SO_4$, > 99.0%, EMSURE), tetrapropylammonium hydroxide (TPAOH, 1 M aq. solution, Alfa Aesar), aluminum sulfate octadecahydrate ($Al_2(SO_4)_3$ $18H_2O$, > 99.9%, Arcos Organics), pyridine ($C_5H_5N$, Merck, EMSURE), aqua regia: a mixture of hydrochloric acid (HCl, fuming 37%, Merck) and nitric acid ($HNO_3$, 65%, Merck, EMSURE) in a ratio 3:1, methanol (Acros, HPLC grade, 99.99% pure), lithium borate (75%, Sigma-Aldrich), $N_2$ (Linde, 99.998%), He (Linde, > 99%), and Ar (Linde, 99.998%). A commercial zeolite ZSM-5 sample (ACS Material) with a $SiO_2/Al_2O_3$ ratio of 38 was used as a reference.

Waste flotation tailings from primary copper (Cu) production were used to extract amorphous silica ($SiO_2$). Two different silica materials, at different pH values (i.e., pH = 3 and pH = 10), with varying the impurities content were extracted. The exact procedure which was followed can be found elsewhere.[26] The silica materials precipitated at pH = 3 and pH = 10 are denoted as S3 and S10, accordingly.

The two different silica materials, derived from the waste stream, were a precursor for the zeolite synthesis. The mass ratio of Si, Al, Na, TPAOH, and $H_2O$ were 1.0:0.05:0.08:0.2:25. $SiO_2$, demineralized water, and sodium hydroxide were mixed and stirred for 2 h at 80 °C. The template (TPAOH) was added and the solution was kept stirring for an additional 2 h. Afterward, the mixture was cooled down, and an Al source (i.e., $Al_2(SO_4)_3 \cdot 18H_2O$) was added and kept stirring for 1 h. The final mixture was put in an autoclave and heated at 175 °C at 48 h. The obtained solid (NaZSM-5) was dried for 12 h at 120 °C in air and calcined for 8 h at 550 °C in air. In order to get the zeolite material in its proton form, the NaZSM-5 was added in 1 M $NH_4NO_3$ for 2.5 h at 80 °C (this step was repeated 2 times). The $NH_4$ZSM-5 first dried for 12 h at 60 °C and then calcined for 4 h at 550 °C in air to obtain the HZSM-5 material. The zeolite synthesized using waste-derived silica materials precipitated at pH = 3 and pH = 10 are denoted as S3 HZSM-5 and S10 HZSM-5, respectively.

Steaming treatments were performed in a quartz tubular oven (Thermoline 79300) using nitrogen ($N_2$) flow going through a bubbler to produce steam at a temperature of 100 °C under ambient pressure. In order to reach the steaming temperature, a ramp was applied of 10 °C/min under $N_2$ flow (100 ml/min) and then an isothermal step was followed at the desired steaming

temperature, while $N_2$ was switched to pass through the bubbler. The steaming temperature was varied from 400 until 700 °C, while the duration of the steaming was varied among 15, 30, 120, and 300 min.

### Materials characterization

Inductively Coupled Plasma-Optical Emission Spectroscopy (ICP-OES) was performed on a SPECTRO CIROS$^{CCD}$ instrument of SPECTRO Analytical Instruments for determining the chemical composition. The samples were prepared by aqua regia and lithium borate. X-ray Diffraction (XRD) was measured on a Bruker D2 X-ray powder diffractometer with Co Kα X-ray tube (λ = 1.7902 Å) as a source. Ammonia Temperature-Programmed Desorption ($NH_3$-TPD) was measured on a Micromeritics AutoChemII 2920. Deconvolution of the $NH_3$-TPD curves was performed applying a Gaussian function using OriginLab. Three different peak positions were chosen and attributed to different types of acid sites (i.e., ~230 °C for weak, ~320 °C for intermediate, and ~435 °C for strong acid sites). The amount of each type of acid sites was calculated based on the area of each Gaussian peak and plotted over steaming time. Pyridine adsorption followed by Fourier-Transform Infrared (FT-IR) spectroscopy was performed using a Bruker Vertex 70v spectrometer in the spectral range of 4000–1000 $cm^{-1}$. Experimental details of these measurements were described elsewhere.[52,61] X-band Electron Paramagnetic Resonance (EPR) was measured using a Bruker EMX plus instrument at 99 K with 100 kHz modulation frequency and 0.25 mT amplitude. The amount of the samples was constant at 80 mg, and the recorded range of the EPR spectra was 0–6000 Gauss (G). Ar physisorption measurements of the catalyst materials were performed using a Micromeritics TriStar 3000 instrument operating at −196 °C. Before performing the measurements, the samples were dried for 15 h at 300 °C under a $N_2$ flow. The morphology of the samples was determined by Scanning Electron Microscopy (SEM) using a FEI Helios Nanolab G3 instrument. Prior to the measurements, samples were coated with a layer of Pt.

### Catalytic testing

The catalytic performance of the samples was tested in an *operando* UV-Vis spectroscopy set-up, which was equipped to perform MTH experiments. ~69 mg of the samples were placed in a fixed-bed reactor using a Weight Hourly Space Velocity (WHSV) of 9 $h^{-1}$ at 350 °C. Methanol and the reaction products were measured by an Interscience Compact Gas Chromatograph (GC). The set-up is equipped with an AvaSpec 2048L spectrometer via a high-temperature UV-Vis optical fiber probe, which enables recording of *operando* UV-Vis Diffuse Reflectance Spectroscopy (DRS) data. More details of the experimental set-up can be found elsewhere.[61,73]

## Acknowledgements

*The authors would like to thank dr. Matteo Monai (Utrecht University) for the valuable feedback. This research has received funding from the European Union's EU Framework Program for Research and Innovation Horizon 2020 under Grant Agreement No. 721385 (MSCA-ETN SOCRATES - https://etn-socrates.eu/).*

## Conflict of Interest

The authors declare no conflict of interest.

## Data Availability Statement

The data that support the findings of this study are available from the corresponding author upon reasonable request.

**Keywords:** Acidity · Methanol-to-Hydrocarbons · steaming · waste valorization · zeolites

[1] R. Anuwattana, K. J. Balkus, S. Asavapisit, P. Khummongkol, *Microporous Mesoporous Mater.* **2008**, *111*, 260–266.
[2] M. I. Epov, N. V. Yurkevich, S. B. Bortnikova, Y. G. Karin, O. P. Saeva, *Russ. Geol. Geophys.* **2017**, *58*, 1543–1552.
[3] P. Altinkaya, J. Liipo, E. Kolehmainen, M. Haapalainen, M. Leikola, M. Lundström, *Mining, Metall. Explor.* **2019**, *36*, 335–342.
[4] Y. R. Lee, J. T. Soe, S. Zhang, J. W. Ahn, M. B. Park, W. S. Ahn, *Chem. Eng. J.* **2017**, *317*, 821–843.
[5] M. Yoldi, E. G. Fuentes-Ordoñez, S. A. Korili, A. Gil, *Microporous Mesoporous Mater.* **2019**, *287*, 183–191.
[6] B. Deka, K. G. Bhattacharyya, *J. Environ. Manage.* **2015**, *150*, 479–488.
[7] E. Saputra, S. Muhammad, H. Sun, H. M. Ang, M. O. Tadé, S. Wang, *Catal. Today* **2012**, *190*, 68–72.
[8] K. Srivastava, V. Devra, A. Rani, *Fuel Process. Technol.* **2014**, *121*, 1–8.
[9] D. Jain, C. Khatri, A. Rani, *Fuel Process. Technol.* **2010**, *91*, 1015–1021.
[10] J. Park, G. D. Saratale, S.-K. Cho, S. Bae, *Sci. Total Environ.* **2020**, *705*, 134544.
[11] S. Vasireddy, A. Campos, E. Miamee, A. Adeyiga, R. Armstrong, J. D. Allison, J. J. Spivey, *Appl. Catal. A* **2010**, *372*, 184–190.
[12] A. Escardino, A. Barba, E. Sanchez, V. Cantavella, *Br. Ceram. Trans.* **1999**, *98*, 172–177.
[13] Y. Huang, X. Chen, Y. Deng, D. Zhou, L. Wang, *Chem. Eng. J.* **2015**, *269*, 434–443.
[14] E. I. Basaldella, R. M. Torres Sánchez, M. S. Conconi, *Appl. Clay Sci.* **2009**, *42*, 611–614.
[15] D. Li, Y. Chen, J. Hu, B. Deng, X. Cheng, Y. Zhang, *Appl. Catal. B* **2020**, *270*, 118881.
[16] F. Ferella, I. D'Adamo, S. Leone, V. Innocenzi, I. De Michelis, F. Vegliò, *Sustain.* **2019**, *11*, DOI 10.3390/su11010113.
[17] F. Ferella, V. Innocenzi, F. Maggiore, *Resour. Conserv. Recycl.* **2016**, *108*, 10–20.
[18] X. Liu, L. Li, T. Yang, Z. Yan, *J. Porous Mater.* **2012**, *19*, 133–139.
[19] E. I. Basaldella, J. C. Paladino, M. Solari, G. M. Valle, *Appl. Catal. B* **2006**, *66*, 186–191.
[20] G. Li, B. Wang, Q. Sun, W. Q. Xu, Z. Ma, H. Wang, D. Zhang, J. Zhou, *Green Energy & Environ.* **2019**, *4*, 470–482; Environ. **2019**, 4, 470–482.
[21] R. N. M. Missengue, P. Losch, G. Sedres, N. M. Musyoka, O. O. Fatoba, B. Louis, P. Pale, L. F. Petrik, *Comptes Rendus Chim.* **2017**, *20*, 78–86.
[22] R. N. M. Missengue, P. Losch, N. M. Musyoka, B. Louis, P. Pale, L. F. Petrik, *Catalysts* **2018**, *8*, 124.
[23] M. Chareonpanich, T. Namto, P. Kongkachuichay, J. Limtrakul, *Fuel Process. Technol.* **2004**, *85*, 1623–1634.
[24] M. Popova, S. Boycheva, H. Lazarova, D. Zgureva, K. Lázár, Á. Szegedi, *Catal. Today* **2020**, *357*, 518–525.
[25] S. Boycheva, D. Zgureva, M. Václavíková, Y. Kalvachev, H. Lazarova, M. Popova, *J. Hazard. Mater.* **2019**, *361*, 374–382.
[26] N. Nikolopoulos, R. G. Geitenbeek, G. T. Whiting, B. M. Weckhuysen, *J. Catal.* **2021**, *396*, 136–147.
[27] Y. Jiang, Y. Wang, W. Zhao, J. Huang, Y. Zhao, G. Yang, Y. Lei, R. Chu, *J. Inst. Chem.* **2016**, *61*, 234–240.
[28] A. J. O'Malley, A. J. Logsdail, A. A. Sokol, C. R. A. Catlow, *Faraday Discuss.* **2016**, *188*, 235–255.
[29] F. Yaripour, Z. Shariatinia, S. Sahebdelfar, A. Irandoukht, *J. Nat. Gas Sci. Eng.* **2015**, *22*, 260–269.
[30] Z. Hu, H. Zhang, L. Wang, H. Zhang, Y. Zhang, H. Xu, W. Shen, Y. Tang, *Catal. Sci. Technol.* **2014**, *4*, 2891–2895.
[31] C. Sun, J. Du, J. Liu, Y. Yang, N. Ren, W. Shen, H. Xu, Y. Tang, *Chem. Commun.* **2010**, *46*, 2671–2673.
[32] R. Wei, C. Li, C. Yang, H. Shan, *J. Nat. Gas Chem.* **2011**, *20*, 261–265.
[33] H. Sharbini Kamaluddin, X. Gong, P. Ma, K. Narasimharao, A. Dutta Chowdhury, M. Mokhtar, *Mater. Today Chem.* **2022**, *26*, 101061.
[34] M. Dusselier, M. A. Deimund, J. E. Schmidt, M. E. Davis, *ACS Catal.* **2015**, *5*, 6078–6085.

[35] M. Rostamizadeh, F. Yaripour, *J. Inst. Chem.* **2017**, *71*, 454–463.
[36] Z. Li, J. Martínez-Triguero, J. Yu, A. Corma, *J. Catal.* **2015**, *329*, 379–388.
[37] S. Zhang, Y. Gong, L. Zhang, Y. Liu, T. Dou, J. Xu, F. Deng, *Fuel Process. Technol.* **2015**, *129*, 130–138.
[38] S. M. T. Almutairi, B. Mezari, E. A. Pidko, P. C. M. M. Magusin, E. J. M. Hensen, *J. Catal.* **2013**, *307*, 194–203.
[39] P. Altinkaya, Z. Wang, I. Korolev, J. Hamuyuni, M. Haapalainen, E. Kolehmainen, K. Yliniemi, M. Lundström, *Miner. Eng.* **2020**, *158*, 106610.
[40] M. S. Oncel, A. Muhcu, E. Demirbas, M. Kobya, *J. Environ. Chem. Eng.* **2013**, *1*, 989–995.
[41] C. A. Cravotta, *Appl. Geochem.* **2008**, *23*, 203–226.
[42] J. N. Louwen, L. Van Eijck, C. Vogt, E. T. C. Vogt, *Chem. Mater.* **2020**, *32*, 9390–9403.
[43] J. Holzinger, P. Beato, L. F. Lundegaard, J. Skibsted, *J. Phys. Chem. C* **2018**, *122*, 15595–15613.
[44] J. Weitkamp, L. Puppe (Eds.), *Catalysis and Zeolites; Fundamentals and Applications, Springer, Berlin*, **1999**.
[45] E. G. Derouane, G. Zelimir, *J. Solid State Chem.* **1986**, *64*, 296–304.
[46] A. Nastro, Z. Gabelica, P. Bodart, J. B. Nagy, *Stud. Surf. Sci. Catal.* **1984**, *19*, 131–137.
[47] A. Nastro, L. B. Sand, *Zeolites* **1983**, *3*, 57–62.
[48] M. Thommes, K. Kaneko, A. V. Neimark, J. P. Olivier, F. Rodriguez-Reinoso, J. Rouquerol, K. S. W. Sing, *Pure Appl. Chem.* **2015**, *87*, 1051–1069.
[49] D. E. De Vos, B. M. Weckhuysen, T. Bein, *J. Am. Chem. Soc.* **1996**, *118*, 9615–9622.
[50] H. W. Huang, H. Zhu, S. H. Zhang, Q. Zhang, C. Y. Li, *J. Fuel Chem. Technol.* **2019**, *47*, 74–83.
[51] Y. Wang, Y. Chang, M. Liu, A. Zhang, X. Guo, *Molecules* **2019**, *24*, 3462.
[52] E. A. Uslamin, B. Luna-Murillo, N. Kosinov, P. C. A. Bruijnincx, E. A. Pidko, B. M. Weckhuysen, E. J. M. Hensen, *Chem. Eng. Sci.* **2019**, *198*, 305–316.
[53] J. Li, D. Han, Z. Zi, T. He, G. Liu, Z. Wang, J. Wu, J. Wu, *Fuel* **2022**, *313*, 122643.
[54] K. Chen, X. Wu, J. Zhao, H. Zhao, A. Li, Q. Zhang, T. Xia, P. Liu, B. Meng, W. Song, X. Zhu, H. Liu, X. Gao, C. Xu, B. Shen, *J. Catal.* **2022**, *413*, 735–750.
[55] M. Ravi, V. L. Sushkevich, J. A. van Bokhoven, *Nat. Mater.* **2020**, *19*, 1047–1056.
[56] S. H. Begum, C. Te Hung, Y. T. Chen, S. J. Huang, P. H. Wu, X. Han, S. Bin Liu, *J. Mol. Catal. A* **2016**, *423*, 423–432.
[57] J. Fermoso, H. Hernando, P. Jana, I. Moreno, J. Přech, C. Choa-Hernández, P. Pizarro, J. M. Coronado, J. Čejka, D. P. Serrano, *Catal. Today* **2016**, *277*, 171–181.
[58] X. Li, S. Liu, X. Zhu, Y. Wang, S. Xie, W. Xin, L. Zhang, L. Xu, *Catal. Lett.* **2011**, *141*, 1498–1505.
[59] I. Yarulina, K. De Wispelaere, S. Bailleul, J. Goetze, M. Radersma, E. Abou-Hamad, I. Vollmer, M. Goesten, B. Mezari, E. J. M. Hensen, J. S. Martínez-Espín, M. Morten, S. Mitchell, J. Perez-Ramirez, U. Olsbye, B. M. Weckhuysen, V. Van Speybroeck, F. Kapteijn, J. Gascon, *Nat. Chem.* **2018**, *10*, 804–812.
[60] I. Yarulina, S. Bailleul, A. Pustovarenko, J. R. Martinez, K. De Wispelaere, J. Hajek, B. M. Weckhuysen, K. Houben, M. Baldus, V. Van Speybroeck, F. Kapteijn, J. Gascon, *ChemCatChem* **2016**, *8*, 3057–3063.
[61] J. Goetze, B. M. Weckhuysen, *Catal. Sci. Technol.* **2018**, *8*, 1632–1644.
[62] S. Müller, Y. Liu, F. M. Kirchberger, M. Tonigold, M. Sanchez-Sanchez, J. A. Lercher, *J. Am. Chem. Soc.* **2016**, *138*, 15994–16003.
[63] M. Jiao, S. Fan, J. Zhang, X. Su, T. S. Zhao, *Catal. Commun.* **2014**, *56*, 153–156.
[64] M. Stöcker, *Microporous Mesoporous Mater.* **1999**, *29*, 3–48.
[65] K. Y. Lee, S. W. Lee, S. K. Ihm, *Ind. Eng. Chem. Res.* **2014**, *53*, 10072–10079.
[66] J. Li, D. Han, T. He, G. Liu, Z. Zi, Z. Wang, J. Wu, *Fuel Process. Technol.* **2019**, *191*, 104–110.
[67] E. Borodina, H. Sharbini Harun Kamaluddin, F. Meirer, M. Mokhtar, A. M. Asiri, S. A. Al-Thabaiti, S. N. Basahel, J. Ruiz-Martinez, B. M. Weckhuysen, *ACS Catal.* **2017**, *7*, 5268–5281.
[68] D. Mores, J. Kornatowski, U. Olsbye, B. M. Weckhuysen, *Chem. Eur. J.* **2011**, *17*, 2874–2884.
[69] V. Van Speybroeck, K. Hemelsoet, K. De Wispelaere, Q. Qian, J. Van der Mynsbrugge, B. De Sterck, B. M. Weckhuysen, M. Waroquier, *ChemCatChem* **2013**, *5*, 173–184.
[70] K. Hemelsoet, Q. Qian, T. De Meyer, K. De Wispelaere, B. De Sterck, B. M. Weckhuysen, M. Waroquier, V. Van Speybroeck, *Chem. Eur. J.* **2013**, *19*, 16595–16606.
[71] F. L. Bleken, K. Barbera, F. Bonino, U. Olsbye, K. P. Lillerud, S. Bordiga, P. Beato, T. V. W. Janssens, S. Svelle, *J. Catal.* **2013**, *307*, 62–73.
[72] M. J. Wulfers, F. C. Jentoft, *ACS Catal.* **2014**, *4*, 3521–3532.
[73] J. Goetze, F. Meirer, I. Yarulina, J. Gascon, F. Kapteijn, J. Ruiz-Martínez, B. M. Weckhuysen, *ACS Catal.* **2017**, *7*, 4033–4046.
[74] D. Fu, O. van der Heijden, K. Stanciakova, J. E. Schmidt, B. M. Weckhuysen, *Angew. Chem. Int. Ed.* **2020**, *59*, 15502–15506; *Angew. Chem.* **2020**, *132*, 15632–15636.
[75] Q. Qian, C. Vogt, M. Mokhtar, A. M. Asiri, S. A. Al-Thabaiti, S. N. Basahel, J. Ruiz-Martínez, B. M. Weckhuysen, *ChemCatChem* **2014**, *6*, 3396–3408.
[76] J. Valecillos, E. Epelde, J. Albo, A. T. Aguayo, J. Bilbao, P. Castaño, *Catal. Today* **2020**, *348*, 243–256.
[77] J. Valecillos, H. Vicente, A. G. Gayubo, A. T. Aguayo, P. Castaño, *J. Catal.* **2022**, *408*, 115–127.
[78] J. Valecillos, Z. Tabernilla, E. Epelde, E. Sastre, A. T. Aguayo, P. Castaño, *Ind. Eng. Chem. Res.* **2020**, *59*, 13892–13905.
[79] H. S. Kamaluddin, S. N. Basahel, K. Narasimharao, M. Mokhtar, *Catalysts* **2019**, *9*, 364.
[80] L. R. Aramburo, E. De Smit, B. Arstad, M. M. Van Schooneveld, L. Sommer, A. Juhin, T. Yokosawa, H. W. Zandbergen, U. Olsbye, F. M. F. De Groot, B. M. Weckhuysen, *Angew. Chem. Int. Ed.* **2012**, *51*, 3616–3619; *Angew. Chem.* **2012**, *124*, 3676–3679.

Manuscript received: August 13, 2022
Revised manuscript received: September 8, 2022
Accepted manuscript online: September 12, 2022
Version of record online: October 11, 2022